Research Square

Preprints are preliminary reports that have not undergone peer review.
They should not be considered conclusive, used to inform clinical practice,
or referenced by the media as validated information.

Pertinaxin, a salivary Kunitz-type protease inhibitor from Simulium pertinax, inhibits factor Xa and impairs plasma coagulation

Lucyana Keity Santana Silva
Instituto Butantan
Fernanda Faria
Instituto Butantan
Paula Andreia Lucas Calabria
Instituto Butantan
Sarah Natalie Cirilo Gimenes
Instituto Butantan
Camila Amaro Caldeira
Instituto Butantan
Thays Duarte de Oliveira
Instituto Butantan
Nathalya Bezerra Soares
Instituto Butantan
Luciana Aparecida Freitas Sousa
Instituto Butantan
Benedito Carlos Prezoto
Instituto Butantan
Geraldo Santana Magalhaes
geraldo.magalhaes@butantan.gov.br
Instituto Butantan

Research Article

Keywords: Kunitz-type inhibitor, Factor Xa, Anticoagulant, Hemostasis, Black fly

Posted Date: November 9th, 2026

DOI: https://doi.org/10.21203/rs.3.rs-11473845/v1

License: This work is licensed under a Creative Commons Attribution 4.0 International License.
Read Full License

Additional Declarations: No competing interests reported.

Abstract

Salivary protease inhibitors are key components of the anti-hemostatic repertoire that enables hematophagous arthropods to maintain blood flow during feeding. Here, we characterized Pertinaxin, a previously unstudied Kunitz-type protease inhibitor identified in the salivary gland transcriptome of *Simulium pertinax*. Pertinaxin displays the conserved structural features of the Kunitz family and shares substantial sequence similarity with other black fly salivary inhibitors. Recombinant Pertinaxin delayed human plasma coagulation in complementary assays and inhibited selected serine proteases, with factor Xa (FXa) emerging as a prominent target. FXa inhibition occurred in the nanomolar range, whereas thrombin was not significantly inhibited and elastase activity was only minimally affected. Kinetic analyses further supported a concentration-dependent inhibitory effect of Pertinaxin on FXa activity. Together, these characterize Pertinaxin as a functionally active salivary Kunitz-type protease inhibitor with anticoagulant activity and expand our understanding of the antihemostatic repertoire of *S. pertinax* and the molecular strategies employed by simuliids during blood feeding.

Introduction

Hematophagous insects represent major vectors of human and animal diseases, and rely on specialized physiological adaptations to achieve successful blood feeding [1]. Over the course of evolution, these insects have developed a sophisticated salivary repertoire capable of counteracting host hemostatic, inflammatory, and immune responses [2].

Black flies (Diptera: Simuliidae) include highly anthropophilic species such as *Simulium pertinax* (*S. pertinax*), an important human-biting species in South America [3]. Like other hematophagous insects, black flies secrete saliva containing bioactive molecules that interfere with host defenses and facilitate blood meal acquisition [4].

To ensure uninterrupted blood feeding, these salivary molecules disrupt hemostasis, a tightly regulated physiological process that maintains blood fluidity under normal conditions while rapidly halting hemorrhage following vascular injury [5, 6]. This defense system relies on a complex cascade of biochemical interactions involving the vascular endothelium, blood platelets, and plasma coagulation proteases [7, 8].

Upon endothelial damage, exposure of tissue factor (TF) initiates the extrinsic coagulation pathway, which converges with the intrinsic pathway at the level of factor X activation [9]. Within the common pathway, activated factor X (FXa) serves as the primary driver of thrombin generation. Following recruitment to anionic phospholipid membranes, FXa assembles with factor Va (FVa) into the prothrombinase complex, thereby markedly enhancing the conversion of prothrombin to thrombin and promoting subsequent fibrin formation [10, 11].

Given its pivotal role in thrombin generation, FXa represents an important target for anticoagulant intervention [12, 13]. Despite the clinical success of direct FXa inhibitors, bleeding remains an important

limitation of anticoagulant therapy, highlighting the continued interest in alternative anticoagulant strategies. Hematophagous organisms, in turn, constitute a rich source of naturally occurring molecules capable of interfering with host hemostasis, including salivary protease inhibitors that act on coagulation factors [1, 14, 15].

Among the diverse components of black fly saliva, Kunitz-type proteins constitute an important class of serine protease inhibitors that interact with target proteases through an exposed reactive-site loop [2, 4]. Salivary Kunitz-domain proteins characterized in simuliids, such as Simukunin from *Simulium vittatum* [14] and Guianensin from *Simulium guianense* [15], have been shown to target FXa and other serine proteases involved in coagulation and inflammation.

Despite the pharmacological potential of black fly salivary proteins, only a limited number of individual salivary protease inhibitors have been biochemically and functionally characterized. In a previous study by our group, transcriptomic profiling of *S. pertinax* salivary glands identified a diverse repertoire of predicted secreted proteins, including several transcripts encoding conserved Kunitz domains [16]. Among these Kunitz-domain sequences, one transcript, designated Pertinaxin (GenBank: PX745386), was selected for heterologous expression and functional characterization. Here, we describe the structural modeling, recombinant production, and detailed biochemical characterization of Pertinaxin with particular emphasis on its effects on human plasma coagulation and serine proteases involved in hemostasis.

Material and methods

Sequence analysis and structural modeling

The Pertinaxin sequence (GenBank: PX745386) was previously identified among ten predicted secreted Kunitz-domain proteins in the *Simulium pertinax* salivary-gland transcriptome [16]. The presence of a signal peptide, the Kunitz domain annotation, and the boundaries of the predicted mature protein were established in that previous transcriptomic study. Accordingly, the previously defined mature Pertinaxin sequence was used in the present work for recombinant expression and subsequent in silico characterization.

For comparative sequence analysis, full-length amino acid sequences of representative and functionally characterized Kunitz-type inhibitors from other *Simulium* species were retrieved from GenBank. Multiple sequence alignment of Pertinaxin with these homologous proteins was performed using ClustalW with default parameters to evaluate sequence conservation, the characteristic cysteine framework of the Kunitz fold, and the putative P1 and P1´reactive-site residues. For a broader comparison of the FXXGGC region, Kunitz-domain sequences from representative culicid mosquitoes were also retrieved from GenBank and aligned over the region spanning the first to the sixth conserved cysteine residue. Physicochemical properties of the mature Pertinaxin sequence, including predicted molecular weight and theoretical isoelectric point, were calculated using ProtParam available through the ExPASy server.

The three-dimensional structure of mature Pertinaxin was predicted with AlphaFold 3 [17] through the AlphaFold Server, using three fixed model seeds and five models per seed (15 in total). Per-residue confidence (pLDDT) and predicted TM-score (pTM) were recorded, inter-model variability was assessed as the mean pairwise Cα RMSD after superposition on residues 1–56, and disulfide geometry was inspected as the Sγ-Sγ distance for each cysteine pair. The highest-ranked model of the first seed was selected for display. Secondary structure was assigned with DSSP (mkdssp 4.2.2) and used to color the cartoon, which was rendered in PyMOL 3.2.0 (open-source build, Schrödinger LLC).

Cloning and expression of Pertinaxin

The gene encoding the mature Pertinaxin protein was cloned into the bicistronic pSUMO$_{Ulp1}$ expression vector [18], which coexpresses the SUMO protease Ulp1 to promote intracellular cleavage and removal of the N-terminal SUMO fusion partner during recombinant protein production. The C-terminal polyhistidine tag was retained in the mature recombinant protein to enable subsequent affinity purification and immunodetection. Briefly, the Pertinaxin coding sequence was amplified by PCR using primers containing *BamHI* and *XhoI* restriction sites. The amplified fragment and the pSUMO$_{Ulp1}$ vector were digested with the corresponding restriction enzymes and subsequently ligated. The ligation mixture was used to transform chemically competent *Escherichia coli* TOP10 cells (Invitrogen), and positive clones were screened by colony PCR. The integrity of the recombinant construct was subsequently confirmed by Sanger sequencing, as previously described [19].

For recombinant protein expression, *E. coli* BL21 Star™ (DE3) cells were transformed with the pSUMO$_{Ulp1}$-Pertinaxin construct. A single colony was inoculated into LB medium supplemented with chloramphenicol (34 µg/mL) and incubated overnight at 30°C with shaking at 180 rpm. The overnight culture was then diluted 1:50 into fresh LB medium containing the same antibiotic and grown under the same conditions to mid-log phase (OD_{600} ≈ 0.6). Recombinant protein expression was induced with isopropyl-β-d-thiogalactopyranoside (IPTG) at a final concentration of 1 mM, followed by incubation for 4 h at 30°C.

Cells were harvested by centrifugation and stored at -20°C until purification. Aliquots collected immediately before and after IPTG induction were analyzed by 13.5% SDS-PAGE under reducing conditions to assess recombinant protein expression.

All procedures involving genetically modified microorganisms were conducted in a biosafety level 2 (P2) facility authorized by the Institutional Biosafety Committee (CIBio) and the Brazilian National Technical Commission on Biosafety (CTNBio), under authorization N^{o}. 6691/2019, dated November 19, 2019.

Purification of Pertinaxin

Bacterial pellets were resuspended in binding buffer (20 mM sodium phosphate, pH 7.4, 500 mM NaCl, 20 mM imidazole) and lysed by ultrasonication on ice. Cell lysates were clarified by centrifugation (10,000×g, 15 min, 4°C), and the soluble fraction was subjected to immobilized metal affinity chromatography (IMAC) on an ÄKTA start™ chromatography system, taking advantage of the C-terminal polyhistidine tag retained in Pertinaxin.

Purification was performed using a 1 mL HisTrap HP column (Cytiva, Marlborough, MA, USA; Cat. No. 17524701). After washing, Pertinaxin was eluted in a stepwise manner with elution buffer containing 20 mM sodium phosphate, 500 mM NaCl, and imidazole at concentrations of 100, 200, 300, 400, 500, and 1,000 mM. Fractions containing Pertinaxin were dialyzed against Tris-buffered saline (20 mM Tris, 150 mM NaCl, pH 7.4). Protein purity and integrity were assessed by 13.5% SDS-PAGE under reducing conditions and proteins were visualized by Coomassie Brilliant Blue staining [19]. Protein concentration was determined in duplicate using the bicinchoninic acid (BCA) assay (Pierce™ Protein Assay Kit), with bovine serum albumin (BSA) as the standard.

Western blot analysis

For immunodetection, proteins were transferred onto a nitrocellulose membrane, using the Trans-Blot® SD Semi-Dry Transfer Cell (Bio-Rad® Laboratories, Hercules, CA, USA) according to the manufacturer's instructions with modifications. The C-terminal polyhistidine tag of Pertinaxin was detected using a mouse monoclonal anti-polyhistidine antibody (Sigma Life Science, Merck Corporation, Darmstadt, Germany) at a 1:1,000 dilution, followed by a horseradish peroxidase-conjugated anti-mouse IgG secondary antibody (Sigma Life Science, Merck Corporation, Darmstadt, Germany) at a 1:1,000 dilution. Immunoreactive bands were visualized using 0.05% (w/v) 4-chloro-1α-naphthol in 15% (v/v) methanol in the presence of 0.03% H_2O_2 (v/v), as previously described [19].

Human plasma collection and preparation

Human blood samples were obtained from healthy adult volunteers (18–60 years old) who provided written informed consent. Peripheral venous blood was collected into tubes containing 3.2% sodium citrate, and platelet-poor plasma (PPP) was prepared by two consecutive centrifugation steps at 2,000 × g for 15 min. The resulting PPP was used for plasma recalcification, prothrombin time (PT), activated partial thromboplastin time (aPTT), and rotational thromboelastometry (ROTEM) assays. All procedures were approved by the Research Ethics Committee of the Butantan Institute through Plataforma Brasil and conducted in accordance with the Declaration of Helsinki (CAAE: 93911025.0.0000.0366).

Recalcification time (RT) assay

The RT assays were performed as previously described by Tsujimoto et al. [14], with minor modifications. Briefly, aliquots (80 µL) of citrated human platelet-poor plasma samples were mixed with

Pertinaxin (20 µL; final concentrations as indicated) and HEPES-buffered saline (40 µL; 150 mM NaCl, 10 mM HEPES, pH 7.4) in a flat-bottom 96-well plate. These mixtures were preincubated at 37°C for 15 min. Coagulation was initiated by the addition of 10 µL of prewarmed 225 mM $CaCl_2$ solution, resulting in a final $CaCl_2$ concentration of 15 mM. Absorbance at 650 nm was immediately monitored at 10-s intervals at 37°C using a SpectraMax 340 microplate reader (Molecular Devices). RT was defined as the time required for the absorbance to reach an OD_{650} of 0.04, corresponding to the increase in turbidity associated with clot formation. Samples that did not reach this threshold within the 2100-s monitoring period were considered not to have clotted within the assay observation window.

Prothrombin time (PT) and activated partial thromboplastin time (aPTT) assays

PT and aPTT assays were performed as previously described by Aounallah et al. [21] and Batista et al. [22] with minor modifications, using commercial kits (STA-PTT Automate 5 for aPTT and STA-Neoplastine® CI Plus for PT) and a semi-automated coagulation analyzer (START STAGO®, Diagnostica Stago).

For the aPTT assays, 30 µL of platelet-poor plasma samples were incubated with STA-PTT Automate 5 reagent (50 µL) in the presence or absence of Pertinaxin (20 µL; final concentrations as indicated) at 37°C. Coagulation was initiated by the addition of 50 µL of 25 mM $CaCl_2$, and aPTT values were recorded by the coagulation analyzer.

For PT assays, 30 µL of platelet-poor plasma samples were incubated with Pertinaxin (20 µL; final concentrations as indicated) at 37°C, followed by the addition of STA-Neoplastine® CI Plus thromboplastin reagent (50 µL) to initiate coagulation. PT values were recorded using the coagulation analyzer.

For PT and aPTT assays, control reactions were performed using the corresponding vehicle buffer in place of Pertinaxin. Recombinant SUMO was tested at a concentration equimolar to the highest Pertinaxin concentration used in each assay to control for nonspecific effects associated with the recombinant-protein preparation.

Rotational thromboelastometry (ROTEM) analysis

ROTEM assays were performed as previously described by Prezoto and Oguiura [23], with minor modifications using human platelet-poor plasma samples and a ROTEM® Delta instrument (Instrumentation Laboratory, Germany). The reaction mixture consisted of 260 µL of human platelet-poor plasma, 20 µL of 200 mM $CaCl_2$, and 60 µL of Tris-HCl buffer with or without Pertinaxin at the indicated concentrations. The clotting time (CT) parameter, defined as the time elapsed from the beginning of the assay until the onset of clot formation, was used as the primary parameter to assess the effect of

Pertinaxin on coagulation [24]. The assay was monitored for up to 3000 s; samples in which clot formation was not detected within this period were considered not to have clotted within the observation window.

Serine protease inhibition screening

The inhibitory activity of Pertinaxin against selected serine proteases was evaluated using chromogenic substrate assays under conditions optimized for each enzyme. The panel comprised trypsin (T1426, Sigma-Aldrich), elastase (E8140, Sigma-Aldrich), human thrombin (Enzyme Research Laboratories, South Bend, IN, USA), plasmin (P1867, Sigma-Aldrich), and human factor Xa (Enzyme Research Laboratories, South Bend, IN, USA).

Each enzyme was preincubated with Pertinaxin at fixed concentrations of 0.5 or 1 μM in 20 mM Tris-HCl, 150 mM NaCl, 0.1% BSA, pH 7.4 for 10 min at 37°C prior to substrate addition. Reactions were initiated by the addition of the corresponding chromogenic substrate: S-2238 (H-D-Phe-Pip-Arg-pNA·2HCl; 0.2 mM) for thrombin, S-2251 (H-D-Val-Leu-Lys-pNA·2HCl; 0.2 mM) for plasmin, and S-2765 (Z-D-Arg-Gly-Arg-pNA·2HCl; 0.2 mM) for FXa, all purchased from Chromogenix (UK); S-4760 (N-succinyl-Ala-Ala-Ala-p-nitroanilide; 2 mM) for elastase and B3133 (Nα-benzoyl-L-arginine 4-nitroanilide hydrochloride; 2 mM) for trypsin were purchased from Sigma-Aldrich.

Substrate hydrolysis was monitored spectrophotometrically over time, and initial reaction velocities (V_0) were determined from the slopes of the linear portions of the kinetic curves by linear regression. Enzymatic activity in the absence of Pertinaxin was defined as 100%, and residual activity in its presence was expressed relative to the corresponding uninhibited control. For proteases substantially inhibited by Pertinaxin, concentration-response assays were performed using increasing inhibitor concentrations. IC_{50} values were determined from normalized enzymatic activities by nonlinear regression using a four-parameter variable-slope [inhibitor] vs. normalized response model in GraphPad Prism 10. The molar inhibitor-to-enzyme ratio at the IC_{50} was calculated as IC_{50}/[enzyme].

FXa inhibition and kinetic characterization

FXa inhibition by Pertinaxin was characterized using the chromogenic substrate S-2765 (Chromogenix), with modifications from previously described methods [25]. Assays were performed in 20 mM Tris-HCl, 150 mM NaCl, 0.1% BSA, pH 7.4 at 37°C using human factor Xa (Enzyme Research Laboratories, South Bend, IN, USA).

For concentration-response analysis, FXa (10 nM, final concentration) was preincubated with increasing concentrations of Pertinaxin (0–12 nM, final concentrations) for 10 min at 37°C. Reactions were initiated by the addition of S-2765 to a final concentration of 200 μM and monitored at 405 nm at 37°C. Initial reaction velocities (V_0) were determined from the linear portion of the progress curves and normalized to the uninhibited control, which was defined as 100% activity. The apparent IC_{50} was determined by

nonlinear regression using a four-parameter variable-slope [inhibitor] versus normalized response model in GraphPad Prism 10.

For kinetic characterization, FXa (4 nM) was assayed with increasing concentrations of S-2765 (20–400 µM) in the absence or presence of Pertinaxin (0, 1, 1.5, and 2 nM). Reactions were performed in a final volume of 100 µL in clear, flat-bottom 96-well microplates at 37°C. Substrate hydrolysis was monitored at 405 nm, and initial reaction velocities (V_0) were determined from the linear portion of the progress curves. Absorbance rates were converted to product formation rates (µM/min) using a molar extinction coefficient for p-nitroaniline of ε_{405} = 9.9 × 10^3 M^{-1} cm^{-1} and an optical path length of 0.37 cm.

Apparent Michaelis-Menten parameters (Km,app and Vmax,app) were obtained by nonlinear regression at each Pertinaxin concentration. The complete data set was additionally analyzed by global nonlinear regression using a classical mixed-inhibition model in GraphPad Prism 10, from which an apparent inhibition constant (Ki,app) and α were obtained. Because the inhibitor concentrations used (1–2 nM) were comparable to or lower than the total FXa concentration (4 nM), inhibitor depletion may become significant under these experimental conditions. Therefore, the fitted constants were treated as apparent parameters and were not used to assign an inhibition mechanism. Lineweaver-Burk and Dixon transformations were generated as complementary descriptive analyses and are provided as supplementary material.

Statistical analysis

Statistical analyses were performed using GraphPad Prism version 10 (GraphPad Software, Boston, MA, USA). Data are presented as mean ± standard deviation (SD). Experiments were performed in technical triplicate, unless otherwise indicated. Comparisons among multiple groups were performed using one-way analysis of variance (ANOVA) followed by Dunnett's or Šídák's multiple-comparisons test, as appropriate and as indicated in the corresponding figure legends. Concentration-response curves were analyzed by nonlinear regression using a four-parameter variable-slope model, and apparent IC_{50} values are reported with their corresponding 95% confidence intervals (CI). FXa kinetic data were analyzed by nonlinear regression as described above, and fitted kinetic parameters are reported with 95% CI where applicable. Differences were considered statistically significant at $p < 0.05$. For coagulation assays in which clot formation was not detected within the predefined observation period, the assay upper limit was used only for graphical representation, and these censored observations were excluded from inferential comparisons of clotting time.

Results

Identification and selection of Kunitz-domain protein

Ten sequences encoding predicted secreted Kunitz-domain proteins were previously identified in the *Simulium pertinax* salivary gland transcriptome [16]. Among them, the most highly expressed transcript was chosen for further investigation. Sequence analysis revealed that this specific transcript shares

72.3% amino acid identity with the mature sequence of Simukunin, a functionally characterized Kunitz inhibitor from *Simulium vittatum* [14]. Given its high expression level and high sequence identity to Simukunin, this sequence was selected for cloning and functional characterization and designated Pertinaxin (accession number PX745386).

The Pertinaxin open reading frame encodes a precursor containing an N-terminal signal peptide (Fig. 1A), with the predicted mature protein having a molecular mass of 9.79 kDa and a theoretical isoelectric point of 9.34. Sequence alignment with the black fly Kunitz inhibitors Sibanin [26], Guianensin [15], and Simukunin [14] revealed six conserved cysteine residues occupying the canonical BPTI positions of the mature protein (Cys5, Cys14, Cys30, Cys38, Cys51 and Cys55), consistent with the disulfide pairing C5–C55, C14–C38 and C30–C51 that defines the Kunitz fold. The alignment also revealed the conserved Kunitz family signature and the putative P_1-P_1' reactive-site residues Arg15-Ala16 (Fig. 1B).

Within the conserved FXXGGC region, Pertinaxin displayed an FEYGGC sequence, differing from the FYYGGC sequence conserved among the other aligned black fly Kunitz inhibitors. Comparison with Kunitz domains from culicid mosquitoes showed additional variation at the two variable positions of this motif, with FTFGGC observed in *C. p. pallens* and *A. aegypti* and FKFGGC in *A. maculipalpis* and *A. funestus* (Supplementary Fig. S2).

The predicted structure displayed the canonical Kunitz architecture, with a two-stranded antiparallel β-hairpin packed against the C-terminal α-helix, the three predicted disulfide bonds consistently observed across all models (Sγ–Sγ distances 1.85–2.11 Å) and Arg15 exposed at the tip of the reactive-site loop (Fig. 1C). Confidence was not uniform along the chain: the conserved Kunitz core (residues 1–56) was predicted with high confidence and was essentially invariant across the fifteen models (mean pLDDT 93.8; mean pairwise Cα RMSD 0.19 Å), whereas the basic C-terminal extension (residues 67–84) was predicted with low confidence and adopted divergent conformations (mean pLDDT below 50; mean pairwise Cα RMSD 15.4 Å after superposition on residues 1–56), indicating that its conformation is not defined by the model.

Expression and purification of Pertinaxin

Recombinant Pertinaxin was expressed in *E. coli* BL21 Star (DE3) using the $pSUMO_{Ulp1}$ expression system [18]. The resulting recombinant protein retained additional vector-derived GS and LE residues alongside a C-terminal 6×His tag (GS-Pertinaxin-LE-6×His), yielding a calculated molecular mass of approximately 11 kDa. SDS-PAGE analysis revealed a predominant band with an apparent molecular mass around 13 kDa (Fig. 2A). Immunoblotting with an anti-His antibody confirmed the presence of the His-tagged recombinant protein at the corresponding apparent molecular mass (Fig. 2B). The purification procedure yielded approximately 0.8 mg of recombinant Pertinaxin per liter of bacterial culture.

Effects of Pertinaxin on human plasma coagulation system

The anticoagulant activity of Pertinaxin was initially evaluated using a human plasma coagulation. Pertinaxin prolonged the RT in a concentration-dependent manner compared with the control (Fig. 3A). At 7 and 14 nM Pertinaxin, clot formation was not observed within the 2100-s monitoring period, and these conditions therefore exceeded the upper observation limit of the assay. In contrast, the recombinant SUMO control did not significantly affect the RT compared with the buffer control.

Pertinaxin produced a concentration-dependent prolongation of both PT and aPTT (Fig. 3B, C). In the PT assay, the highest Pertinaxin concentration tested (0.3 μM) reached the upper observation limit of the assay (#), whereas lower concentrations produced measurable prolongation of clotting time. The recombinant SUMO control did not significantly alter either PT or aPTT compared with the corresponding buffer control.

Figure 3 Effect of Pertinaxin on plasma coagulation. (A) Plasma recalcification time in the presence of buffer alone (Control), recombinant SUMO (14 nM), or Pertinaxin (0.85-14 nM). (B) Prothrombin time (PT) and (C) activated partial thromboplastin time (aPTT) in the presence of Control, recombinant SUMO [0.3 μM (PT) or 1.5 μM (aPTT)], or increasing concentrations of Pertinaxin. Conditions marked with # did not clot within the respective assay monitoring period and are displayed at the upper observation limit for graphical representation. Results are expressed as mean ± SD of triplicates. Statistical significance was assessed by ordinary one-way ANOVA followed by Dunnett's multiple-comparisons test versus the respective control; conditions marked with # were excluded from the statistical analysis. *$p < 0.05$, ****$p < 0.0001$; ns, not significant

The anticoagulant effect of Pertinaxin was further evaluated by rotational thromboelastometry (ROTEM) using calcium-triggered plasma coagulation. Pertinaxin delayed the initiation of clot formation, as evidenced by a concentration-dependent prolongation of the CT parameter compared with the control (Fig. 4). At 0.75 and 1 μM Pertinaxin, no clot formation was detected within the 3000-s observation period. These findings were consistent with the conventional plasma coagulation assays and further demonstrated a concentration-dependent anticoagulant effect in human plasma.

Screening of serine protease inhibition

The inhibitory activity of Pertinaxin was initially evaluated against a panel of serine proteases, including elastase, thrombin, plasmin, trypsin, and FXa (Fig. 5). Pertinaxin exhibited a distinct inhibitory profile among the proteases tested. Thrombin activity was not significantly affected at any of the concentrations tested, whereas elastase showed a modest but significant reduction in residual activity. In contrast, Pertinaxin markedly reduced the residual activities of plasmin, trypsin, and FXa at both concentrations tested. Plasmin retained only a small fraction of its activity, while trypsin and FXa activities were nearly abolished under the screening conditions.

Figure 5 Inhibitory activity of Pertinaxin against selected serine proteases. The inhibitory activity of Pertinaxin was evaluated against elastase, thrombin, plasmin, trypsin, and factor Xa (FXa) at inhibitor concentrations of 0.5 and 1 μM. Enzyme activity was determined from the initial reaction rates obtained by linear regression of the linear portion of the kinetic curves and normalized to the respective control reaction performed in the absence of Pertinaxin, which was defined as 100% activity. Results are expressed as residual enzyme activity (%) and presented as mean ± SD of triplicates. Statistical comparisons were performed separately for each enzyme using one-way ANOVA followed by Šídák's multiple-comparisons test, comparing each Pertinaxin concentration with its respective control *p < 0.05, **p < 0.01, ****p < 0.0001; ns, not significant

Based on the marked reduction in residual activity observed for plasmin, trypsin, and FXa, concentration–response assays were performed to further characterize the inhibitory potency of Pertinaxin against these enzymes (Table 1). Pertinaxin inhibited all three proteases in a concentration-dependent manner, with apparent IC_{50} values of 6.17 nM for FXa (95% CI: 5.8–6.4 nM), 40.13 nM for trypsin (95% CI: 36.76–43.06 nM), and 82.3 nM for plasmin (95% CI: 71.4–94.6 nM), determined at enzyme concentrations of 10, 60, and 10 nM, respectively. The corresponding IC_{50}/[enzyme] molar ratios were 0.617, 0.669, and 8.23, respectively. For FXa and trypsin, these ratios were below unity, indicating that the inhibitor concentration required for half-maximal inhibition was of the same order as the enzyme concentration present in the assay. Under such conditions, the apparent IC_{50} is influenced by the enzyme concentration and therefore should not be interpreted as a direct measure of inhibitor affinity. For plasmin, in contrast, the inhibitor was in molar excess over the enzyme. Accordingly, the values in Table 1 are reported as assay-dependent apparent IC_{50} values and should not be interpreted as direct affinity constants.

Table 1

Apparent IC_{50} values of Pertinaxin against selected serine proteases. Values were obtained by nonlinear regression of normalized residual enzyme activity at the indicated enzyme concentrations. The IC_{50}/[enzyme] molar ratio is provided to indicate the relationship between inhibitor potency and the enzyme concentration used in each assay

Enzyme	Enzyme (nM)	Apparent IC_{50} (nM)	95% CI (nM)	IC_{50}/[enzyme]
Factor Xa	10	6.17	5.8–6.4	0.617
Trypsin	60	40.13	36.76–43.06	0.669
Plasmin	10	82.3	71.4–94.6	8.23

Table 1
Apparent IC_{50} values of Pertinaxin against selected serine proteases.

Enzyme	Enzyme (nM)	Apparent IC_{50} (nM)	95% CI (nM)	IC_{50}/[enzyme]
Factor Xa	10	6.17	5.8–6.4	0.617
Trypsin	60	40.13	36.76–43.06	0.669
Plasmin	10	82.3	71.4–94.6	8.23

Given its low-nanomolar apparent IC_{50} and its pivotal role in coagulation, FXa was therefore selected for further characterization of Pertinaxin-mediated inhibition.

Concentration-dependent inhibition of FXa amidolytic activity

The concentration-dependent inhibition of FXa by Pertinaxin was subsequently examined in greater detail (Fig. 6). Progress curves showed a progressive reduction in S-2765 hydrolysis with increasing Pertinaxin concentrations (Fig. 6A). At 10 and 12 nM Pertinaxin, FXa activity was nearly completely abolished under the assay conditions.

Initial reaction rates derived from the linear portion of the progress curves were normalized to the control and used to generate a concentration-response curve (Fig. 6B). Pertinaxin inhibited FXa in a concentration-dependent manner, yielding an apparent IC_{50} of 6.17 nM (95% CI: 5.8–6.4 nM) under these assay conditions.

Figure 6 Concentration-dependent inhibition of FXa by Pertinaxin. (A) Progress curves of FXa-mediated substrate hydrolysis in the absence (Control) or presence of increasing concentrations of Pertinaxin (3–12 nM), monitored by absorbance at 405 nm. The first 10 min of the reaction progress curves are shown. (B) Concentration-response curve for FXa inhibition by Pertinaxin. Initial reaction rates were determined from the slopes of the linear portion of the progress curves and normalized to the control in the absence of Pertinaxin, defined as 100% activity. Concentration-response data were fitted by nonlinear regression to determine the half-maximal inhibitory concentration (IC_{50}), yielding an apparent IC_{50} of 6.17 nM under these assay conditions (95% CI: 5.8–6.4 nM). Data are expressed as mean ± SD

To further characterize the effect of Pertinaxin on FXa catalysis, substrate saturation curves were obtained at fixed inhibitor concentrations. Increasing concentrations of Pertinaxin produced a progressive decrease in apparent Vmax, while apparent Km values remained comparatively stable (Fig. 7; Table S1).

Global nonlinear regression of the complete data set to a classical mixed-inhibition model yielded an apparent K_i of 2.65 nM (95% CI: 1.97–3.83 nM) and a fitted α of 1.119 (95% CI: 0.667–1.793) (Table 2). The 95% confidence interval for α encompassed unity, indicating that the fitted behavior was compatible with the noncompetitive limit of the mixed-inhibition model.

Table 2

Apparent kinetic parameters for FXa inhibition by Pertinaxin. Parameters were obtained by global nonlinear regression of substrate-saturation data (S-2765, 20–400 μM) obtained with 4 nM FXa in the presence of Pertinaxin (0–2 nM), using a classical mixed-inhibition model. Values are reported as best-fit estimates with their corresponding 95% confidence intervals

Parameter	Best-fit value	95% CI
Apparent Vmax (μM min^{-1})	6.994	6.699–7.318
Apparent Km (μM)	106.7	94.30-120.9
Apparent Ki (nM)	2.65	1.97–3.83
α	1.119	0.667–1.793

Table 2

Apparent kinetic parameters for FXa inhibition by Pertinaxin.

Parameter	Best-fit value	95% CI
Vmax (μM min^{-1})	6.994	6.699–7.318
Km (μM)	106.7	94.30–120.9
Ki (nM)	2.65	1.97–3.83
α	1119	0.667–1.793

Because the Pertinaxin concentrations used in these experiments (1–2 nM) were comparable to or lower than the total FXa concentration (4 nM), inhibitor depletion may influence the observed kinetic behavior. Accordingly, the fitted parameters were considered apparent values and were not used to assign a specific inhibition mechanism. Lineweaver–Burk and Dixon transformations are presented as complementary descriptive analyses in Figure S1.

Discussion

Kunitz-type protease inhibitors are recurrent components of the salivary repertoire of hematophagous arthropods and contribute to the modulation of host hemostatic and inflammatory pathways [27, 28]. Here, we characterized Pertinaxin, a previously uncharacterized Kunitz-domain protein identified in the salivary gland transcriptome of *S. pertinax* [16]. Pertinaxin prolonged coagulation in complementary plasma-based assays and inhibited selected serine proteases, with a particularly pronounced effect on factor Xa (FXa). These findings expand the repertoire of functionally characterized Kunitz inhibitors from black flies and support FXa as an important target of simuliid salivary anti-hemostatic activity. The conserved cysteine framework, predicted disulfide bonds, and surface-exposed reactive-site loop identified in Pertinaxin are consistent with the structural organization characteristic of Kunitz-type

protease inhibitors [27, 29]. Its mature sequence shares 72.3% amino acid identity with Simukunin from *S. vittatum* [14].

Recombinant Pertinaxin was obtained as a soluble protein using the $pSUMO_{Ulp1}$ vector developed in our laboratory [18]. Following intracellular SUMO removal, its calculated molecular mass was approximately 11 kDa, whereas SDS-PAGE showed an apparent mass of approximately 13 kDa. Differences between calculated and electrophoretic molecular mass have been frequently reported for proteins displaying anomalous migration in SDS-PAGE and may result from factors such as amino acid composition,charge distribution or incomplete SDS binding [30, 31]. Immunodetection of the C-terminal His tag at the same apparent molecular mass further supported the identification of this band as recombinant Pertinaxin.

Pertinaxin prolonged human plasma RT, PT, aPTT, and the CT parameter measured by ROTEM, demonstrating a consistent anticoagulant effect under different experimental conditions. The magnitude of the effect differed among assays, which is consistent with their distinct modes of coagulation activation and analytical conditions. Prolongation of both PT and aPTT is compatible with interference at or downstream of the convergence of the intrinsic and extrinsic coagulation pathways, although these assays alone cannot identify the molecular target [32].

The protease-screening experiments provided additional mechanistic context, as FXa was strongly inhibited whereas thrombin activity was not significantly affected. A similar profile has been reported for Simukunin and Guianensin, which inhibit FXa without detectable inhibition of thrombin [14, 15]. Guianensin also prolongs PT and aPTT and interferes with prothrombinase activity [15]. Thus, the plasma phenotype observed for Pertinaxin is compatible with an effect upstream of thrombin generation, with FXa representing a plausible contributor to its anticoagulant activity. Pertinaxin, however, was not restricted to FXa. It also inhibited trypsin and plasmin, whereas elastase was only minimally affected. Because different enzyme concentrations were required in these assays, inhibitory affinity cannot be directly ranked solely from the apparent IC_{50} values.

Comparison with other characterized simuliid Kunitz proteins reveals distinct differences in their protease-inhibition profiles. Simukunin strongly inhibits both FXa and elastase [14], while Sibanin binds both enzymes with nanomolar affinity [26], and Guianensin displays a broader inhibitory spectrum [15]. These differences, despite conservation of the Kunitz scaffold, are consistent with the functional diversity of this inhibitor family and suggest that sequence variation within the conserved Kunitz scaffold may contribute to differences in protease recognition [27].

Interestingly, Pertinaxin differs from the other aligned simuliid Kunitz inhibitors within the otherwise conserved FXXGGC region, displaying FEYGGC instead of FYYGGC. Although the functional significance of this substitution remains unknown, variations in residues outside the reactive site of Kunitz inhibitors have been shown to influence scaffold-loop organization [28] and protease recognition [29]. Thus, the Tyr-to-Glu substitution observed in Pertinaxin could contribute to local structural or electrostatic differences that influence protease recognition, a possibility that will require experimental validation.

Targeted structure-function studies will be required to identify the residues responsible for the distinct specificity of Pertinaxin.

Given its pronounced inhibition in the initial screening and its central role in coagulation, Pertinaxin-mediated FXa inhibition was further characterized by kinetic analysis,with an apparent IC_{50} of 6.17 nM in the concentration-response analysis and a fitted apparent Ki of 2.65 nM in the substrate-saturation experiments. Increasing Pertinaxin concentrations reduced apparent Vmax with comparatively smaller changes in apparent Km, demonstrating a marked effect on FXa catalytic activity. However, the inhibitor concentrations used in the kinetic experiments (1–2 nM) were comparable to or lower than the total FXa concentration (4 nM). Under such conditions, enzyme-inhibitor complex formation can significantly reduce the concentration of free inhibitor, limiting the applicability of classical inhibition models [33].

The kinetic parameters obtained here should therefore be regarded as apparent values, and neither the mixed-model fit nor the Lineweaver-Burk and Dixon transformations are sufficient to assign a definitive inhibition mechanism. This caution is particularly relevant under tight-binding conditions, in which inhibitor depletion can substantially affect kinetic parameter estimates obtained with classical inhibition models [33, 34]. Simukunin, for example, binds FXa with nanomolar affinity, whereas Guianensin forms a high-affinity complex with catalytically accessible FXa [14, 15]. Direct binding measurements or kinetic approaches accounting for inhibitor depletion will be required to establish the intrinsic affinity and mechanism of the Pertinaxin-mediated FXa interaction.

The identification of FXa inhibition in Pertinaxin adds to accumulating evidence that targeting this coagulation protease is a recurrent feature of the anti-hemostatic repertoire of black flies. Anti-FXa activity has been detected in salivary gland extracts from different *Simulium* species [35], and individual salivary Kunitz inhibitors, including Simukunin, Guianensin, and Sibanin, have subsequently been shown to target FXa [14, 15, 26].

Together with these observations, the anticoagulant and enzymatic activities of Pertinaxin support the view that Kunitz-type inhibitors contribute to the molecular diversity through which black flies interfere with host coagulation during blood feeding. At the same time, differences in protease specificity among these inhibitors indicate that conservation of the Kunitz scaffold does not necessarily imply equivalent functional profiles. Further characterization of the Pertinaxin-FXa interaction, particularly through direct binding and structure-function studies, will be important to define its intrinsic affinity, molecular determinants of protease recognition, and contribution to the anti-hemostatic activity of *S. pertinax* saliva.

Conclusion

This study provides the functional characterization of Pertinaxin, a salivary Kunitz-type protease inhibitor from *S. pertinax*. Recombinant Pertinaxin impaired human plasma coagulation in complementary assays and inhibited selected serine proteases, with a particularly pronounced effect on FXa. Its inhibitory profile, characterized by marked inhibition of FXa, trypsin, and plasmin, limited activity toward elastase,

and no significant effect on thrombin, differs from those reported for other characterized simuliid Kunitz inhibitors and highlights the functional diversity of this protein family. Kinetic analyses confirmed concentration-dependent inhibition of FXa activity, although the inhibition constants should be regarded as apparent and do not permit definitive assignment of an inhibition mechanism. Together, these findings identify Pertinaxin as a functionally active salivary anticoagulant and support FXa inhibition as an important contributor to its anti-hemostatic activity. Further studies on the Pertinaxin-FXa relationship and the structural determinants of protease recognition will help clarify its biological function.

Declarations

Competing Interests

The authors have no relevant financial or non-financial interests to disclose.

Ethics approval

This study was performed in accordance with the Declaration of Helsinki and was approved by the Research Ethics Committee of the Butantan Institute (CAAE: 93911025.0.0000.0366).

Consent to publish

Not applicable.

Funding

C.A.C., and T.D.O. received research support from the FAPESP (grant numbers 2021/11206-5, and 2023/11334-9, respectively). L.K.S.S. received research support from CAPES (grant number 88887.924162/2023-00), and FAPESP (grant number 2020/08863-1 and 2025/04421-8)

Author Contribution

LKSS conceived and designed the experimental work, performed the experiments, analyzed and interpreted the data, and wrote the original draft of the manuscript. FF contributed to the prothrombin time and activated partial thromboplastin time assays and provided reagents for the enzymatic assays. PALC and CAC contributed to molecular cloning and heterologous protein expression. SNCG contributed to the kinetic analyses. TDdeO assisted with the bioinformatics analyses. NBS contributed to the purification of the recombinant protein. LAFdeS contributed to the standardization and analysis of the plasma recalcification assay. BCP contributed to the ROTEM assay and provided the reagents required for its performance. GSM conceived the study, acquired funding, provided resources, supervised the

project, and critically reviewed and edited the manuscript. All authors reviewed and approved the final manuscript.

Acknowledgement

The authors gratefully acknowledge all colleagues and collaborators who contributed to the development of this study through technical assistance, scientific discussions, and valuable comments and suggestions throughout the course of this work.

References

1. Ribeiro JMC, Francischetti IMB (2003) Role of arthropod saliva in blood feeding: sialome and post-sialome perspectives. Annu Rev Entomol 48:73–88. https://doi.org/10.1146/annurev.ento.48.060402.102812
2. Chmelar J, Calvo E, Pedra JHF, Francischetti IMB, Kotsyfakis M (2012) Tick salivary secretion as a source of antihemostatics. J Proteom 75:3842–3854. https://doi.org/10.1016/j.jprot.2012.04.026
3. Gil-Azevedo LH, Maia-Herzog M (2004) Diagnostic characters of *Simulium (Chirostilbia) pertinax* Kollar (Diptera: Simuliidae). Neotrop Entomol 33:433–437
4. Andersen JF, Pham VM, Meng Z, Champagne DE, Ribeiro JMC (2009) An insight into the sialome of the black fly, *Simulium vittatum*. J Proteome Res 8:1474–1488. https://doi.org/10.1021/pr8008429
5. Hoffman M, Monroe DM III (2001) A cell-based model of hemostasis. Thromb Haemost 85:958–965. https://doi.org/10.1055/s-0037-1615947
6. Versteeg HH, Heemskerk JWM, Levi M, Reitsma PH (2013) New fundamentals in hemostasis. Physiol Rev 93:327–358. https://doi.org/10.1152/physrev.00016.2011
7. Furie B, Furie BC (2008) Mechanisms of thrombus formation. N Engl J Med 359:938–949. https://doi.org/10.1056/NEJMra0801082
8. Gale AJ (2011) Continuing education course #2: current understanding of hemostasis. Toxicol Pathol 39:273–280. https://doi.org/10.1177/0192623310389474
9. Palta S, Saroa R, Palta A (2014) Overview of the coagulation system. Indian J Anaesth 58:515–523. https://doi.org/10.4103/0019-5049.144643
10. Mackman N (2008) Triggers, targets and treatments for thrombosis. Nature 451:914–918. https://doi.org/10.1038/nature06797
11. Schreuder M, Reitsma PH, Bos MHA (2019) Blood coagulation factor Va's key interactive residues and regions for prothrombinase assembly and prothrombin binding. J Thromb Haemost 17:1229–1239. https://doi.org/10.1111/jth.14487
12. Weitz JI (2007) Factor Xa or thrombin: is factor Xa a better target? J Thromb Haemost 5(Suppl 1):60–64. https://doi.org/10.1111/j.1538-7836.2007.02473.x

13. Becker RC (2021) Factor Xa inhibitors: critical considerations for clinical development and testing. J Thromb Thrombolysis 51:959–968. https://doi.org/10.1007/s11239-021-02455-x
14. Tsujimoto H, Kotsyfakis M, Francischetti IMB, Eum JH, Strand MR, Champagne DE (2012) Simukunin from the salivary glands of the black fly *Simulium vittatum* inhibits enzymes that regulate clotting and inflammatory responses. PLoS ONE 7:e29964. https://doi.org/10.1371/journal.pone.0029964
15. Valenzuela-Leon PC, Campos Chagas A, Martin-Martin I, Williams AE, Berger M, Shrivastava G, Paige AS, Kotsyfakis M, Tirloni L, Calvo E (2023) Guianensin, a *Simulium guianense* salivary protein, has broad anti-hemostatic and anti-inflammatory properties. Front Immunol 14:1163367. https://doi.org/10.3389/fimmu.2023.1163367
16. Caldeira CA, Silva LKS, de Oliveira TD, de Barros Pinto Viviani Cunha A, Viala VL et al (2026) Sialotranscriptome of *Simulium pertinax* and functional characterization of SpVaP: a novel recombinant simuliid-specific vasodilator. Mol Cell Biochem. https://doi.org/10.1007/s11010-026-05718-4. de Carvalho Lins Fernandes Távora B
17. Abramson J, Adler J, Dunger J et al (2024) Accurate structure prediction of biomolecular interactions with AlphaFold 3. Nature 630:493–500. https://doi.org/10.1038/s41586-024-07487-w
18. Shimokawa-Falcão LHAL, Caporrino MC, Barbaro KC, Della-Casa MS, Magalhães GS (2017) Toxin fused with SUMO tag: a new expression vector strategy to obtain recombinant venom toxins with easy tag removal inside the bacteria. Toxins (Basel) 9:82. https://doi.org/10.3390/toxins9030082
19. Ferraz KF, De Lucca Caetano LH, Orefice DP, Calabria PAL, Della-Casa MS, Freitas-de-Sousa LA, Beraldo-Neto E, Sanabani SS, Magalhães GS, Clissa PB (2024) Bicistronic vector expression of recombinant Jararhagin-C and its effects on endothelial cells. Toxins (Basel) 16:524. https://doi.org/10.3390/toxins16120524
20. Calabria PAL, Shimokava-Falcao LHAL, Colombini M, Moura-da-Silva AM, Barbaro KC, Faquim-Mauro EL, Magalhaes GS (2019) Design and production of a recombinant hybrid toxin to raise protective antibodies against *Loxosceles* spider venom. Toxins (Basel) 11:108. https://doi.org/10.3390/toxins11020108
21. Aounallah H, Fessel MR, Goldfeder MB, Carvalho E, Bensaoud C, Chudzinski-Tavassi AM, Bouattour A, M'ghirbi Y, Faria F (2021) Rdromaserpin: a novel anti-hemostatic serpin from the salivary glands of the hard tick *Hyalomma dromedarii*. Toxins (Basel) 13:913. https://doi.org/10.3390/toxins13120913
22. Batista IFC, Ramos OHP, Ventura JS, Junqueira-de-Azevedo ILM, Ho PL, Chudzinski-Tavassi AM (2010) A new factor Xa inhibitor from *Amblyomma cajennense* with a unique domain composition. Arch Biochem Biophys 493:151–156. https://doi.org/10.1016/j.abb.2009.10.009
23. Prezoto BC, Oguiura N (2020) Factor XII-deficient chicken plasma as a useful target for screening of pro- and anticoagulant animal venom toxins. Toxins (Basel) 12:79. https://doi.org/10.3390/toxins12020079
24. Whiting D, DiNardo JA (2014) TEG and ROTEM: technology and clinical applications. Am J Hematol 89:228–232. https://doi.org/10.1002/ajh.23599

25. Branco VG, Iqbal A, Alvarez-Flores MP, Sciani JM, de Andrade SA, Iwai LK et al (2016) Amblyomin-X having a Kunitz-type homologous domain, is a noncompetitive inhibitor of FXa and induces anticoagulation in vitro and in vivo. Biochim Biophys Acta 1864:1428–1435. https://doi.org/10.1016/j.bbapap.2016.07.011
26. He Y, Li Z, Wei L, Wang Z, Shen Y, Wang X, Yang X, Mu L, Yang H, Wu J (2025) Sibanin, a novel black fly-derived Kunitz protease inhibitor, prevents thrombus formation in mice by anticoagulation-antiplatelet duality. Int J Biol Macromol 296:139766. https://doi.org/10.1016/j.ijbiomac.2025.139766
27. Ranasinghe S, McManus DP (2013) Structure and function of invertebrate Kunitz serine protease inhibitors. Dev Comp Immunol 39:219–227. https://doi.org/10.1016/j.dci.2012.10.005
28. Khamrui S, Majumder S, Dasgupta J, Dattagupta JK, Sen U (2010) Identification of a novel set of scaffolding residues that are instrumental for the inhibitory property of Kunitz (STI) inhibitors. Protein Sci 19(3):593–602. https://doi.org/10.1002/pro.338
29. Patil DN, Chaudhary A, Sharma AK, Tomar S, Kumar P (2012) Structural basis for dual inhibitory role of tamarind Kunitz inhibitor (TKI) against factor Xa and trypsin. FEBS J 279(24):4547–4564. https://doi.org/10.1111/febs.12042
30. Graceffa P, Jancsó A, Mabuchi K (1992) Modification of acidic residues normalizes sodium dodecyl sulfate-polyacrylamide gel electrophoresis of caldesmon and other proteins that migrate anomalously. Arch Biochem Biophys 297:46–51. https://doi.org/10.1016/0003-9861(92)90639-E
31. Matsumoto H, Haniu H, Komori N (2019) Determination of protein molecular weights on SDS-PAGE. Methods Mol Biol 1855:101–105. https://doi.org/10.1007/978-1-4939-8793-1_10
32. Park S, Park JK (2024) Back to basics: the coagulation pathway. Blood Res 59:35. https://doi.org/10.1007/s44313-024-00040-8
33. Morrison JF (1969) Kinetics of the reversible inhibition of enzyme-catalysed reactions by tight-binding inhibitors. Biochim Biophys Acta 185:269–286. https://doi.org/10.1016/0005-2744(69)90420-3
34. Delfín J, Martínez I, Antuch W, Morera V, González Y, Rodríguez de la Vega M et al (2021) Reviewing the experimental and mathematical factors involved in tight binding inhibitors Ki values determination: the bi-functional protease inhibitor SmCI as a test model. Biochimie 181:86–95. https://doi.org/10.1016/j.biochi.2020.11.014
35. Jacobs JW, Cupp EW, Sardana M, Friedman PA (1990) Isolation and characterization of a coagulation factor Xa inhibitor from black fly salivary glands. Thromb Haemost 64:235–238

Figures

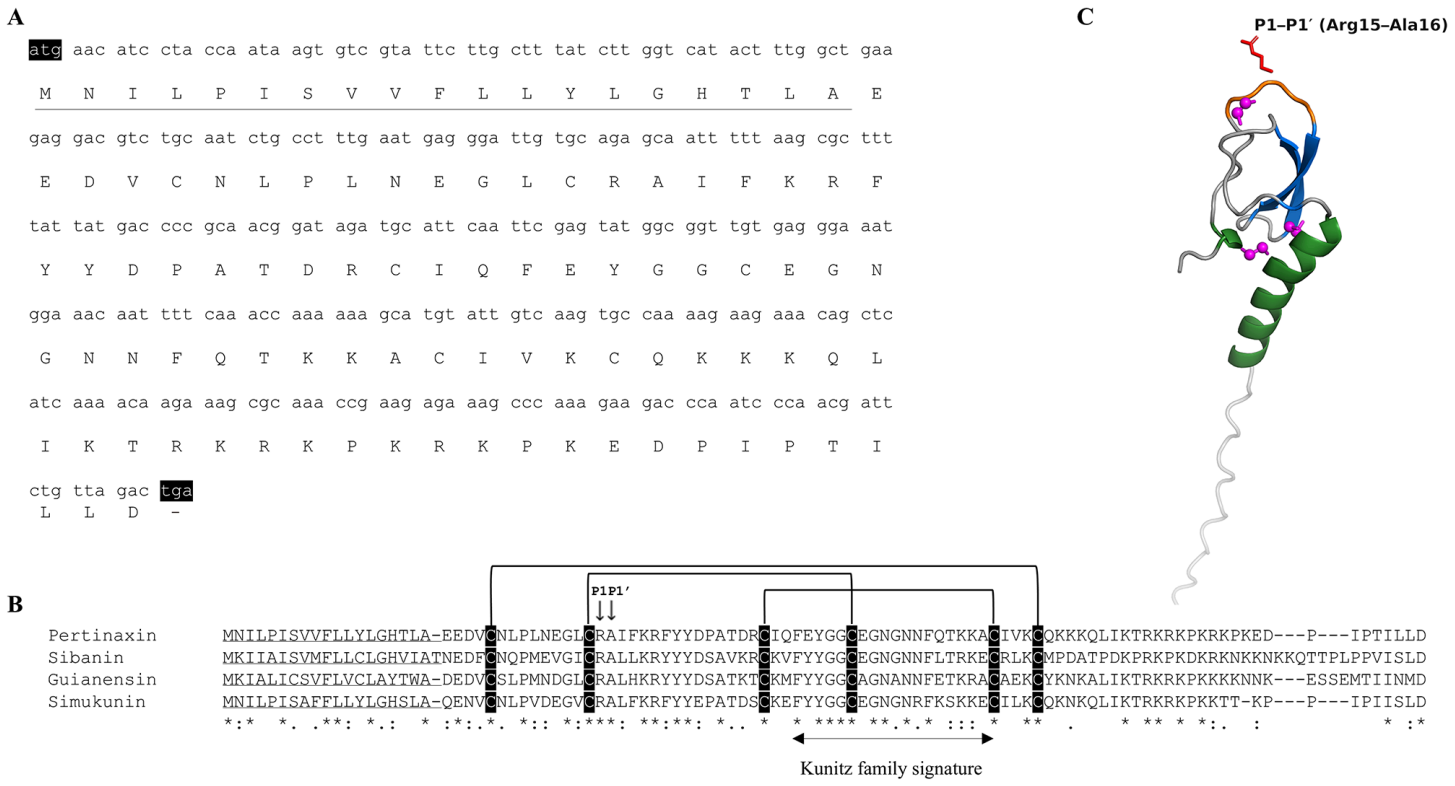


Figure 1

Sequence analysis, predicted three-dimensional structure, and multiple sequence alignment of Pertinaxin. (A) Nucleotide and deduced amino acid sequence of Pertinaxin. Start (ATG) and stop (TGA) codons are highlighted in black, and the predicted N-terminal signal peptide is underlined. (B) Multiple sequence alignment of Pertinaxin with single-domain Kunitz protease inhibitors from Simulium spp. Black boxes indicate the six conserved cysteine residues, with connecting lines representing the predicted disulfide-bond framework. Arrowheads indicate the putative P_1 and P'_1 reactive-site residues, and the double-headed arrow indicates the Kunitz family signature. Identical residues (*), strongly conserved substitutions (:), and weakly conserved substitutions (.) are indicated according to Clustal notation. (C) Predicted three-dimensional structure of mature Pertinaxin. The α-helix (residues 48-66) is shown in green, the antiparallel β-hairpin (residues 18-24 and 29-35) in blue, and loops and coil in grey. Side chains of the six cysteines forming the disulfide bonds Cys5-Cys55, Cys14-Cys38 and Cys30-Cys51 are shown as magenta sticks with the sulfur atoms as spheres. The reactive-site loop is shown in orange, with Arg15 (P1) in red. Residues 67-84 are drawn semi-transparent to indicate low prediction confidence. Residue numbering refers to a mature protein, as in (b)

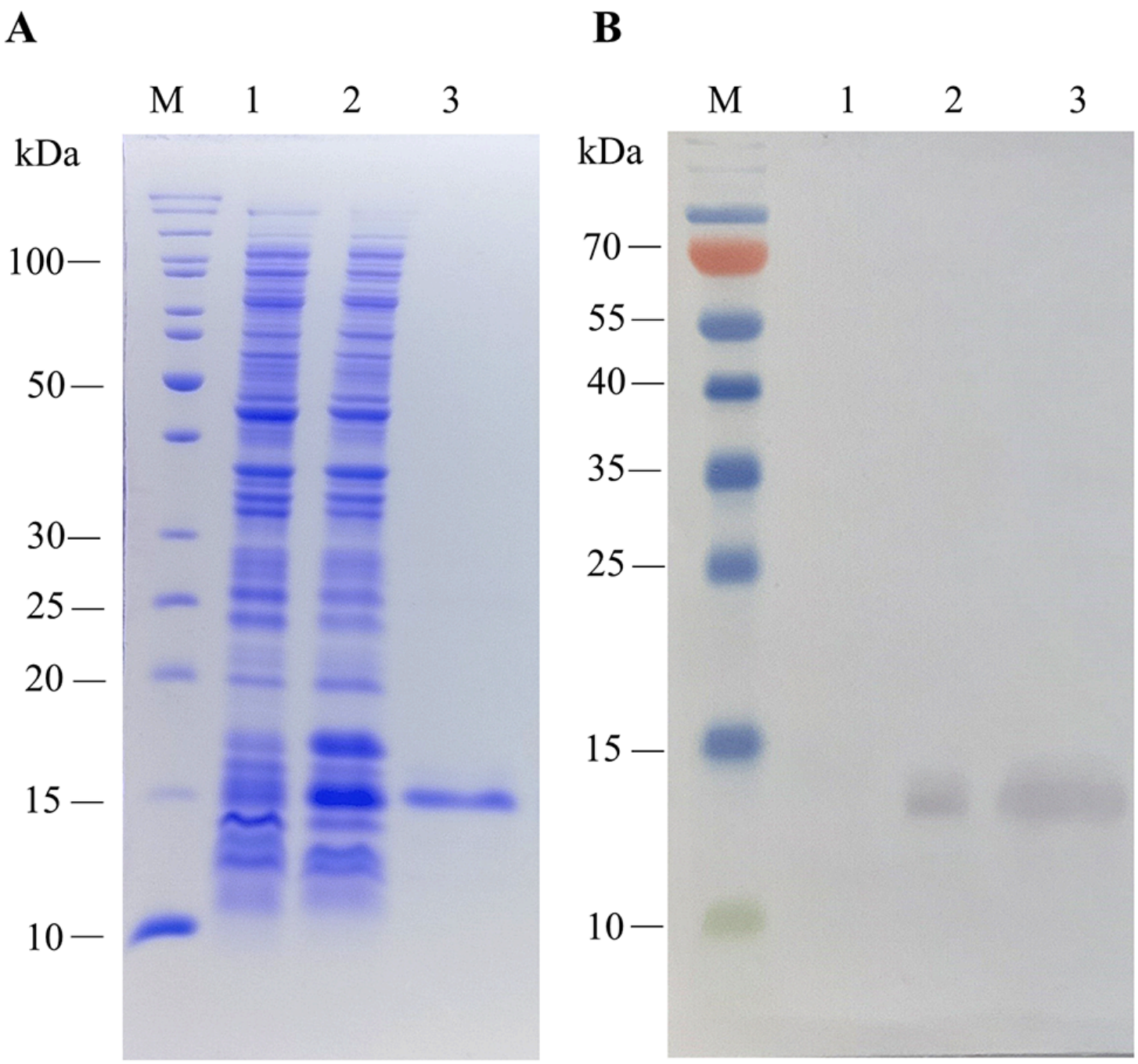


Figure 2

Expression and purification of recombinant Pertinaxin. (A) SDS-PAGE analysis of recombinant Pertinaxin expression in Escherichia coli BL21 Star (DE3) and the purified protein. A predominant band corresponding to recombinant Pertinaxin was observed at an apparent molecular mass of approximately 13 kDa. (B) Western blot analysis using an anti-His antibody for detection of His-tagged recombinant Pertinaxin. M, molecular mass marker; 1, non-induced bacterial extract; 2, IPTG-induced bacterial extract; 3, purified recombinant Pertinaxin

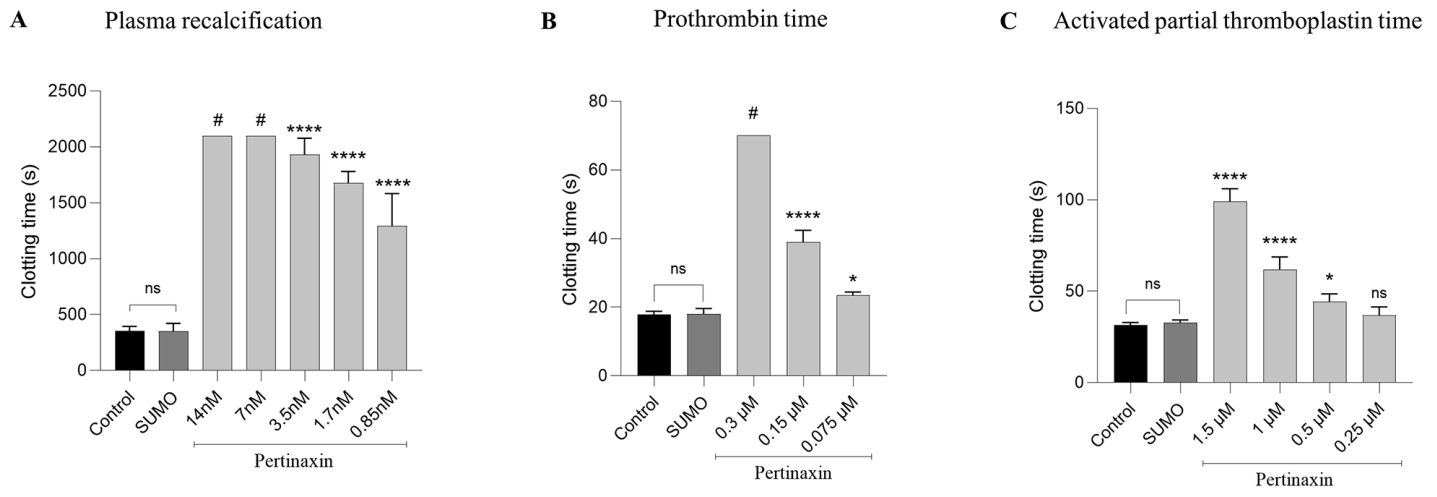


Figure 3

Effect of Pertinaxin on plasma coagulation. (A) Plasma recalcification time in the presence of buffer alone (Control), recombinant SUMO (14 nM), or Pertinaxin (0.85-14 nM). (B) Prothrombin time (PT) and (C) activated partial thromboplastin time (aPTT) in the presence of Control, recombinant SUMO [0.3 µM (PT) or 1.5 µM (aPTT)], or increasing concentrations of Pertinaxin. Conditions marked with # did not clot within the respective assay monitoring period and are displayed at the upper observation limit for graphical representation. Results are expressed as mean ± SD of triplicates. Statistical significance was assessed by ordinary one-way ANOVA followed by Dunnett's multiple-comparisons test versus the respective control; conditions marked with # were excluded from the statistical analysis. *p < 0.05, ****p < 0.0001; ns, not significant

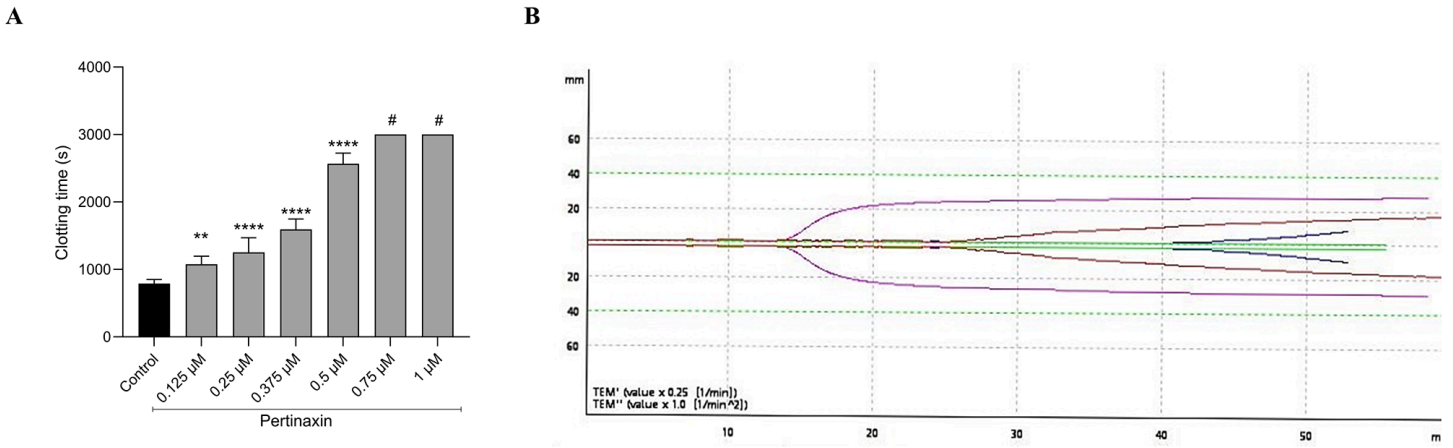


Figure 4

Effect of Pertinaxin on plasma coagulation assessed by rotational thromboelastometry (ROTEM). (A) Clotting time (CT) measured in the absence (Control) or presence of increasing concentrations of Pertinaxin (0.125-1 µM). Results are expressed as mean ± SD of triplicates. Statistical significance was assessed by ordinary one-way ANOVA followed by Dunnett's multiple-comparisons test, with each

Pertinaxin concentration compared with the control. **p < 0.01; ****p < 0.0001. #, no clot formation was detected within the 3000-s observation period. For graphical representation, these conditions are shown at the assay upper limit of 3000 s and were not treated as measured CT values in the statistical analysis. (B) Representative ROTEM traces showing the concentration-dependent delay in clot formation induced by Pertinaxin. The pink curve represents the control (plasma without inhibitor), while the red, blue, and green curves correspond to samples incubated with Pertinaxin at concentrations of 0.25 μM, 0.5 μM, and 0.75 μM, respectively. The x-axis represents the analysis time (minutes) while the y-axis represents the clot amplitude in millimeters (mm).

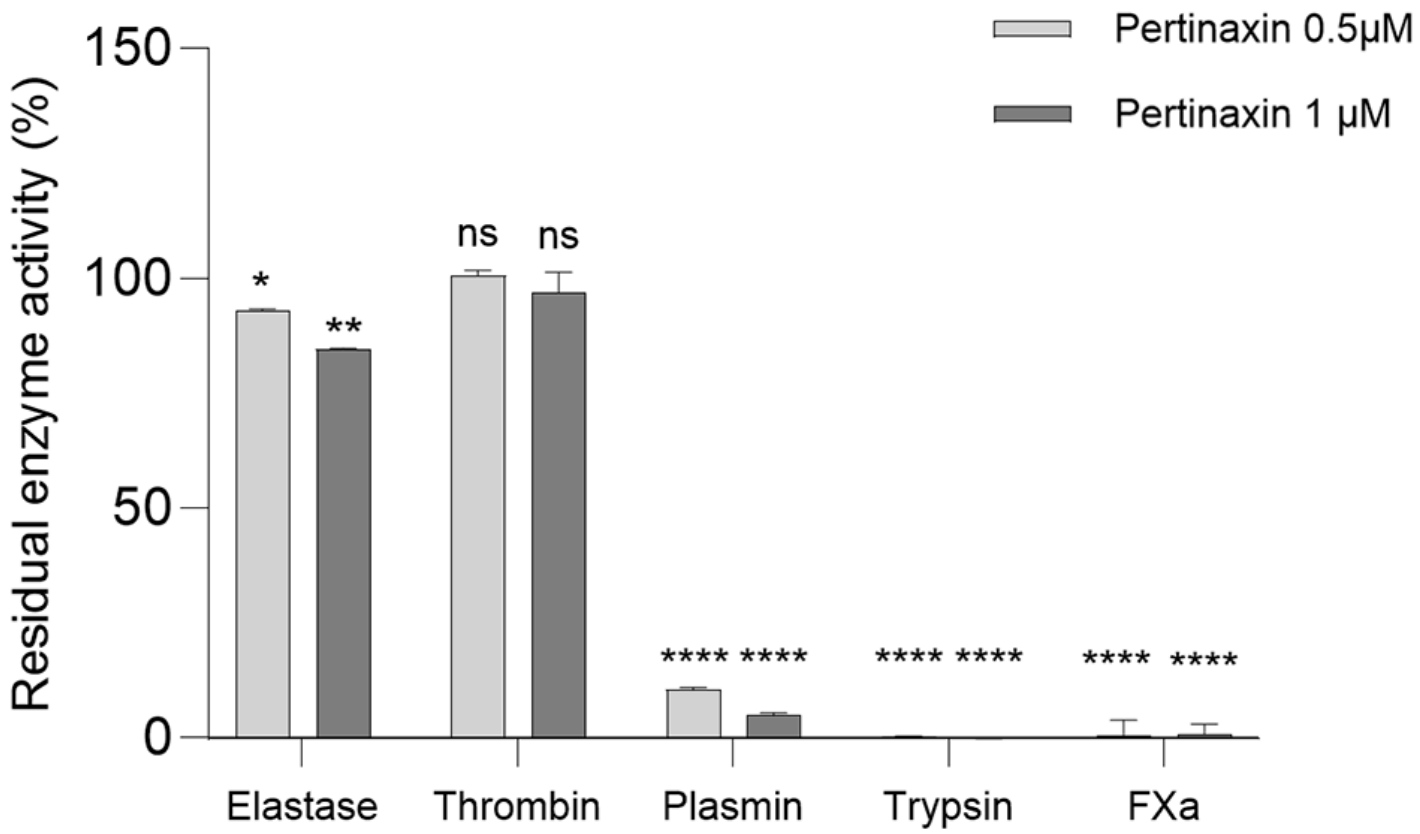


Figure 5

Inhibitory activity of Pertinaxin against selected serine proteases. The inhibitory activity of Pertinaxin was evaluated against elastase, thrombin, plasmin, trypsin, and factor Xa (FXa) at inhibitor concentrations of 0.5 and 1 μM. Enzyme activity was determined from the initial reaction rates obtained by linear regression of the linear portion of the kinetic curves and normalized to the respective control reaction performed in the absence of Pertinaxin, which was defined as 100% activity. Results are expressed as residual enzyme activity (%) and presented as mean ± SD of triplicates. Statistical comparisons were performed separately for each enzyme using one-way ANOVA followed by Šídák's multiple-comparisons test, comparing each Pertinaxin concentration with its respective control *p < 0.05, **p < 0.01, ****p < 0.0001; ns, not significant

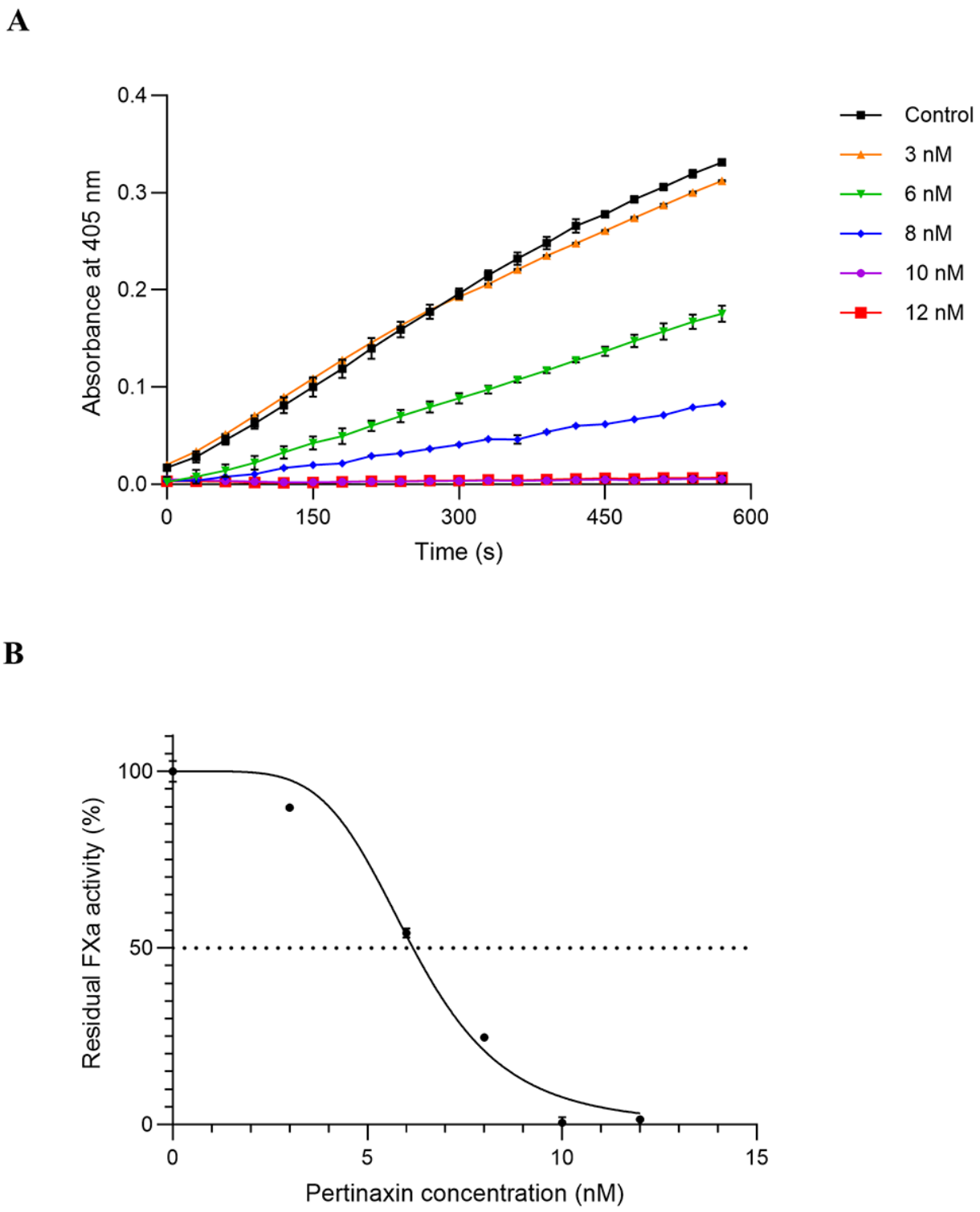


Figure 6

Concentration-dependent inhibition of FXa by Pertinaxin. (A) Progress curves of FXa-mediated substrate hydrolysis in the absence (Control) or presence of increasing concentrations of Pertinaxin (3-12 nM), monitored by absorbance at 405 nm. The first 10 min of the reaction progress curves are shown. (B) Concentration-response curve for FXa inhibition by Pertinaxin. Initial reaction rates were determined from the slopes of the linear portion of the progress curves and normalized to the control in the absence

of Pertinaxin, defined as 100% activity. Concentration-response data were fitted by nonlinear regression to determine the half-maximal inhibitory concentration (IC_{50}), yielding an apparent IC_{50} of 6.17 nM under these assay conditions (95% CI: 5.8 - 6.4 nM). Data are expressed as mean ± SD

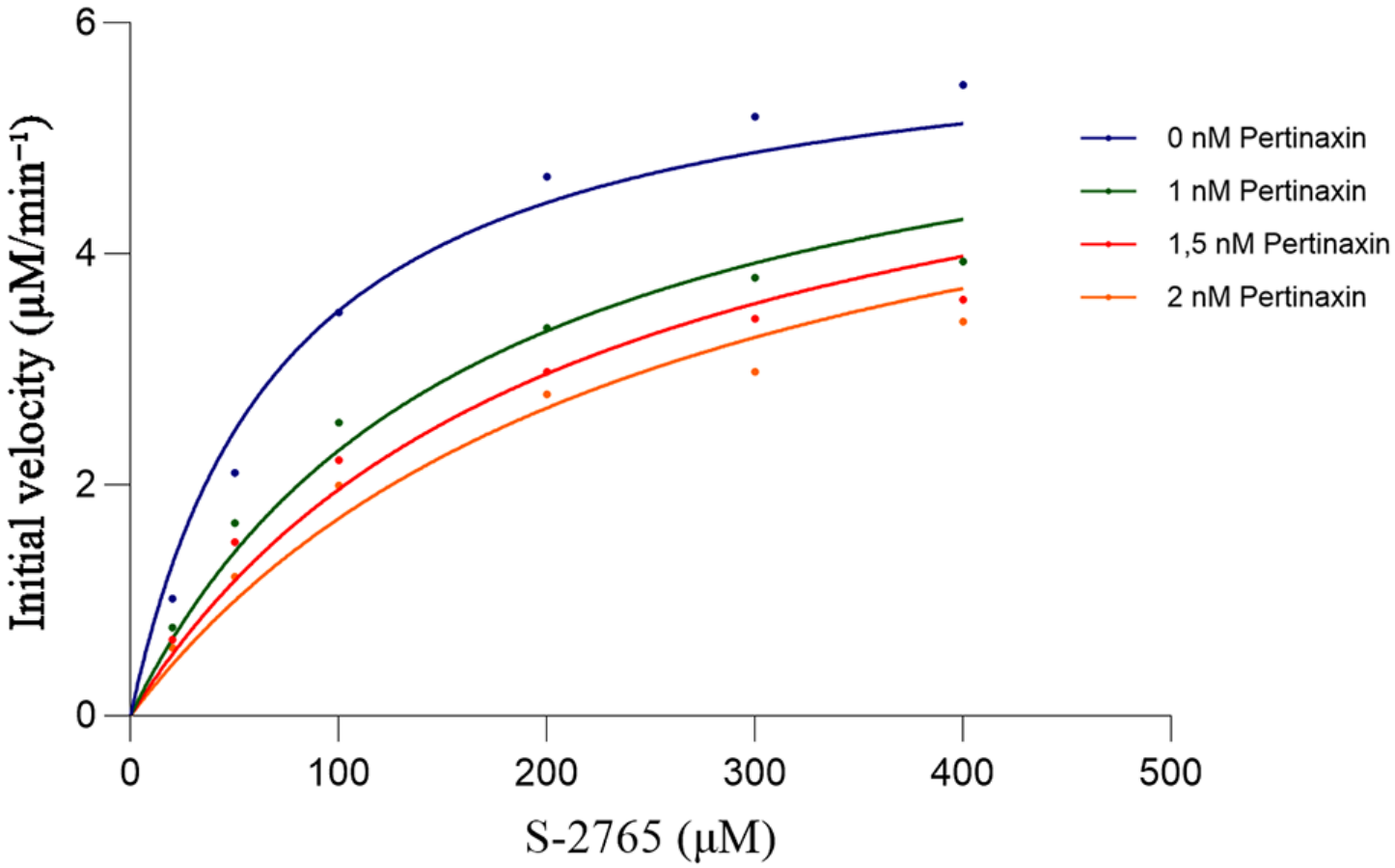


Figure 7

Michaelis–Menten analysis of FXa inhibition by Pertinaxin. Initial velocities of FXa-mediated S-2765 hydrolysis were determined over a range of substrate concentrations in the absence or presence of increasing concentrations of Pertinaxin (1-2 nM). Data were fitted by nonlinear regression to the Michaelis-Menten equation. Increasing Pertinaxin concentrations progressively reduced the reaction velocity. Data are expressed as mean ± SD

Supplementary Files

This is a list of supplementary files associated with this preprint. Click to download.

- SupplementaryInformation.docx